

Polar bulges and polar nuclear discs: the case of NGC 4698

E. M. Corsini,^{1,2,*} J. Méndez-Abreu,^{3,4} N. Pastorello,^{1,5} E. Dalla Bontà,^{1,2}
L. Morelli,^{1,2} A. Beifiori,⁶ A. Pizzella^{1,2} and F. Bertola^{1,2}

¹*Dipartimento di Fisica e Astronomia ‘G. Galilei’, Università di Padova, vicolo dell’Osservatorio 3, I-35122 Padova, Italy*

²*INAF–Osservatorio Astronomico di Padova, vicolo dell’Osservatorio 5, I-35122 Padova, Italy*

³*Instituto Astrofísico de Canarias, Calle Vía Láctea s/n, E-38200 La Laguna, Spain*

⁴*Departamento de Astrofísica, Universidad de La Laguna, Calle Astrofísico Francisco Sánchez, E-38205 La Laguna, Spain*

⁵*Centre for Astrophysics and Supercomputing, Swinburne University of Technology, Hawthorn, VIC 3122, Australia*

⁶*Max-Planck-Institut für extraterrestrische Physik, Giessenbachstraße, D-85748 Garching bei München, Germany.*

Accepted 2012 March 20. Received 2012 March 19; in original form 2011 December 23

ABSTRACT

The early-type spiral NGC 4698 is known to host a nuclear disc of gas and stars which is rotating perpendicularly with respect to the galaxy main disc. In addition, the bulge and main disc are characterised by a remarkable geometrical decoupling. Indeed they appear elongated orthogonally to each other. In this work the complex structure of the galaxy is investigated by a detailed photometric decomposition of optical and near-infrared images. The intrinsic shape of the bulge was constrained from its apparent ellipticity, its twist angle with respect to the major axis of the main disc, and the inclination of the main disc. The bulge is actually elongated perpendicular to the main disc and it is equally likely to be triaxial or axisymmetric. The central surface brightness, scalelength, inclination, and position angle of the nuclear disc were derived by assuming it is infinitesimally thin and exponential. Its size, orientation, and location do not depend on the observed passband. These findings support a scenario in which the nuclear disc is the end result of the acquisition of external gas by the pre-existing triaxial bulge on the principal plane perpendicular to its shortest axis and perpendicular to the galaxy main disc. The subsequent star formation either occurred homogeneously all over the extension of the nuclear disc or through an inside-out process that ended more than 5 Gyr ago.

Key words: galaxies: bulges – galaxies: formation – galaxies: individual: NGC 4698 – galaxies: photometry – galaxies: spiral – galaxies: structure.

1 INTRODUCTION

Several mechanisms have been proposed for bulge assembly. Bulges formed either before the disc by hierarchical merging, or at the same time in a monolithic collapse, or after the disc as a result of secular evolution. Furthermore, there is evidence that bulges can experience accretion events via infall of external material or satellite galaxies. None of these scenarios alone is able to reproduce the observed properties of all the bulges along the Hubble sequence since bulges are a class of diverse and heterogeneous objects. The large bulges of lenticulars and early-type spirals are similar to low-luminosity elliptical galaxies, whereas the small bulges of late-type spirals are reminiscent of disc components (see Kormendy & Kennicutt 2004 and references therein).

The study of the intrinsic shape of bulges is a key constraint on their formation. Although the kinematics of many bulges is well

described by dynamical models of oblate ellipsoids which are flattened by rotation with little or no anisotropy (e.g., Pignatelli et al. 2001; Cappellari et al. 2006), the twisting of the bulge isophotes (Lindblad 1956; Zaritsky & Lo 1986), the presence of non-circular gas motions (e.g., Coccato et al. 2004; Falcón-Barroso et al. 2006), and the misalignment between the major axes of the bulge and disc (Bertola, Vietri, & Zeilinger 1991; Méndez-Abreu et al. 2008, hereafter MA+08) observed in several galaxies cannot be explained if the bulge and disc are both axisymmetric. These features are interpreted as the signature of bulge triaxiality. Perfect axisymmetry is ruled out when the intrinsic shape of bulges is determined by statistical analyses based on their observed ellipticity (Fathi & Peletier 2003, MA+08). A large fraction of bulges are characterised by an elliptical equatorial cross-section, and most of them are flattened along the polar axis they share with the surrounding disc. As a consequence, triaxial bulges elongated perpendicularly with respect to the disc are expected to be very rare (Méndez-Abreu et al. 2010, hereafter MA+10). To date

* E-mail: enricomaria.corsini@unipd.it

NGC 4698 (Bertola et al. 1999), NGC 4672 (Sarzi et al. 2000), and UGC 10043 (Matthews & de Grijs 2004) are the only spiral galaxies known to host a prominent bulge sticking out from the plane of the disc.

We decided to revisit the case of NGC 4698 since such a rare galaxy represents an excellent test case to derive the intrinsic shape of the bulge by applying the method of MA+10. NGC 4698 is an Sab(s) spiral (de Vaucouleurs et al. 1991, hereafter RC3) in the Virgo Cluster. Its total B -band magnitude is $B_T = 11.46$ mag (RC3), which corresponds to $M_B = -19.69$ mag assuming a distance of 17 Mpc (Freedman et al. 1994). The inner region of the large elliptical-like bulge is elongated perpendicular to the major axis of the main disc, i.e. it is a polar bulge; this is also true for the outer parts of the bulge if a parametric photometric decomposition is adopted (Bertola et al. 1999). At the same time, the stellar (Bertola et al. 1999; Corsini et al. 1999) and ionised-gas (Bertola & Corsini 2000) components are characterised by an inner velocity gradient and a central zero-velocity plateau along the minor and major axes of the disc, respectively. This kinematically-decoupled core is rotating perpendicularly with respect to the galaxy main disc. It corresponds to a nuclear stellar disc (hereafter NSD; Pizzella et al. 2002). The geometrical and kinematical orthogonal decoupling of NGC 4698 can hardly be explained without invoking the acquisition of external material from the galaxy outskirts (see Bertola & Corsini 2000).

In this Letter, we improve the previous results by quantitatively constraining the intrinsic shape of the bulge of NGC 4698 in Section 2. The analysis of a near-infrared (NIR) image from the United Kingdom Infrared Telescope (UKIRT) allows us to map the mass distribution and minimise the contamination from dust. We get a more reliable estimate of the galaxy's structural parameters with respect to Bertola et al. (1999) since they folded the eastern side of their optical image around the galaxy major axis to deal with the strongest dust lanes of the main disc. In addition, they assumed the galaxy surface brightness to be the sum of a de Vaucouleurs bulge and an exponential disc *with* orthogonal major axes. Here, no *a priori* choice is made about the orientation of the bulge. The structure of the NSD detected by Pizzella et al. (2002) is analysed in Section 3 in greater detail. The photometric decomposition of multi-band optical images of the galaxy nucleus obtained with the *Hubble Space Telescope* (*HST*) allows us to investigate the formation process of the NSD by studying its stellar populations. Our findings are discussed in Section 4.

2 THE BULGE

2.1 United Kingdom Infrared Telescope imaging

A K -band image of NGC 4698 is available in the first data release of the Large Area Survey of UKIRT Infrared Deep Sky Survey (UKIDSS, Lawrence et al. 2007). It was obtained on 23 January 2007 with a total exposure time of 40 s. The 3.8-m UKIRT telescope is operated in Mauna Kea Observatory (Hawaii, USA). It mounted the Wide Field Camera (WFCAM) with four Rockwell Hawaii-II devices. Each of them consists of 2048×2048 HgCdTe detectors of $18 \times 18 \mu\text{m}^2$ and covers a field of view of $13.7 \times 13.7 \text{ arcmin}^2$ with an image scale of $0.4 \text{ arcsec pixel}^{-1}$. The gain and read-out noise were $4.5 e^- \text{ count}^{-1}$ and $25 e^- \text{ rms}$, respectively. The image was reduced, cleaned for cosmic rays, sky subtracted, and flux calibrated with the WFCAM pipeline (Hambly et al. 2008). A two-dimensional fit with a circular Gaus-

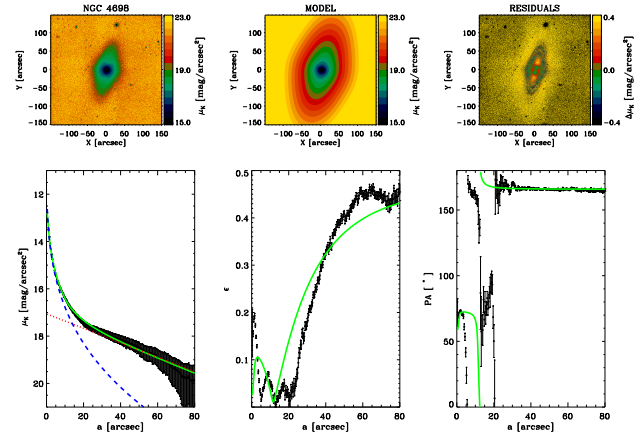


Figure 1. Two-dimensional photometric decomposition of NGC 4698. Top row: UKIDSS K -band image (left-hand panel), best-fit image (central panel), and residual (i.e., observed-model) image (right-hand panel). North is up and East is left. Bottom row: Ellipse-averaged radial profiles of the surface brightness (left-hand panel), ellipticity (central panel), and position angle (right-hand panel) measured in the UKIDSS (dots) and model image (green continuous line). The dashed blue and dotted red lines represent the intrinsic surface-brightness radial profiles of the bulge and main disc, respectively.

sian to the field stars in the resulting image yielded a FWHM = 0.76 arcsec .

The photometric decomposition of the WFCAM image of NGC 4698 was performed using the Galaxy Surface Photometry Two-Dimensional Decomposition (GASP2D) algorithm by MA+08, which yields the structural parameters for a Sérsic bulge and an exponential main disc.

The fitting algorithm relies on a χ^2 minimisation of the intensities in counts, for which we must adopt initial trial parameters that are as close as possible to their final values. The trial values of the effective surface brightness, effective radius, shape parameter, position angle, and axial ratio of the bulge (I_e , r_e , n , PA_b , and q_b) and of the central surface brightness, scalelength, position angle, and axial ratio of the main disc (I_0 , h , PA_d , and q_d) were estimated from the analysis of the ellipse-averaged radial profiles of surface brightness μ_K , ellipticity ϵ , and position angle PA . The latter were measured using the IRAF task ELLIPSE and analysed by following the prescriptions of MA+08. Starting from these initial trial parameters the different photometric models of the surface brightness were fitted iteratively to the galaxy image. Each image pixel was weighted according to the variance of its total observed photon counts due to the contribution of both galaxy and sky, and determined assuming photon noise limitation and taking the detector read-out noise into account. Seeing effects were also taken into account by convolving the model image with a circular Gaussian point spread function (PSF) with a FWHM matching the observed one. The convolution was performed as a product in Fourier domain before the least-squares minimisation. Only the image pixels with an intensity larger than 0.5 times the sky standard deviation were included in the fit. Foreground stars were masked and excluded from the fit. The result of the photometric decomposition is shown in Fig. 1. The residual image shows the tightly-wound spiral arms aligned with the disc major axis. Nevertheless, the fit was satisfactory. The model surface brightness is consistent with the data within the error bars. The differences of ellipticity and position angle between the observed and model isophotes are smaller than 0.1

and 3° , respectively. The PA is scattered in the radial range between about 5 and 20 arcsec where the isophotes are nearly round.

The errors on the fitted parameters were estimated through Monte Carlo simulations on images of artificial galaxies. A set of disc galaxies with a Sérsic bulge and an exponential main disc with $7 < K_T < 8$ mag to bracket the magnitude of NGC 4698 ($K_T = 7.54$ mag, Kassin, de Jong, & Pogge 2006) was generated. The artificial galaxies were assumed to be observed at the distance of the Virgo Cluster taking into account resolution effects. The parameters of the artificial galaxies were randomly chosen in the ranges observed for nearby S0/a-Sb galaxies by Möllenhoff & Heidt (2001). Finally, a background level and photon noise were added to the simulated images in order to mimic the instrumental setup and signal-to-noise of the WFCAM image. The relative errors in the fitted parameters of the artificial galaxies were estimated by comparing the input and output values and were assumed to be normally distributed. The standard deviation was adopted as the 1σ error in the relevant parameter for the bulge-disc decomposition. The best-fitting values and their 3σ errors are $\mu_e = 17.07 \pm 0.64$ mag arcsec $^{-2}$, $r_e = 11.5 \pm 6.0$ arcsec, $n = 3.46 \pm 0.42$, $PA_b = 72^\circ.8 \pm 0^\circ.9$, and $q_b = 0.88 \pm 0.03$ for the bulge, and $\mu_0 = 17.06 \pm 0.72$ mag arcsec $^{-2}$, $h = 35.4 \pm 18.0$ arcsec, $PA_d = 165^\circ.7 \pm 6^\circ.6$, and $q_d = 0.47 \pm 0.06$ for the main disc.

Systematic errors given by a wrong estimation of the PSF FWHM and sky level are the most significant contributors to the error budget, since the spiral arms do not affect the result and no further component is observed. We estimated a 3σ error of 2 and 1 per cent for the sky level and PSF FWHM, respectively. We analysed the artificial galaxies by adopting the correct sky level and a PSF FWHM that was 2 per cent larger (or smaller) than the actual one or the correct PSF FWHM and a sky level that was 1 per cent larger (or smaller) than the actual one. To derive the intrinsic shape of the bulge we are interested in q_b , q_d , PA_b , and PA_d . Their 3σ errors including systematics are smaller than 15 per cent.

2.2 Intrinsic shape of the bulge

The method developed by MA+10 was applied to derive the intrinsic shape of the bulge of NGC 4698. It is based upon the geometrical relationships between the projected and intrinsic shapes of the bulge and its surrounding disc. The bulge is assumed to be a triaxial ellipsoid with semi-axes of length A and B in the equatorial plane and C along the polar axis. The bulge shares the same centre and polar axis as its main disc, which is circular and lies on the equatorial plane of the bulge. The intrinsic shape of the bulge is recovered from the bulge ellipticity parameter $e = (1 - q_b^2)/(1 + q_b^2) = 0.13$, the twist angle $\delta = 180^\circ - |PA_b - PA_d| = 87^\circ.1$ between the major axes of the bulge and main disc (i.e., the line of nodes), and the main disc inclination $\theta = \arccos q_d = 61^\circ.7$.

The relation between the intrinsic and projected parameters depends only on the spatial position of the bulge, i.e., on the angle $0 \leq \phi \leq 90^\circ$ measured on the bulge equatorial plane between the principal axis corresponding to A and the line of nodes. The equatorial ellipticity $Z = B^2/A^2$ and intrinsic flattening $F = C^2/A^2$ of the bulge are given by:

$$\frac{\sin(2\phi_C) \sin^2 \theta}{\cos^2 \theta} F = -\sin \phi_B \cos(2\phi_C - \phi_B) (1 + Z)^2 + \sin(2\phi_C - \phi_B) \sqrt{(1 - Z)^2 - \sin^2 \phi_B (1 + Z)^2}, \quad (1)$$

where:

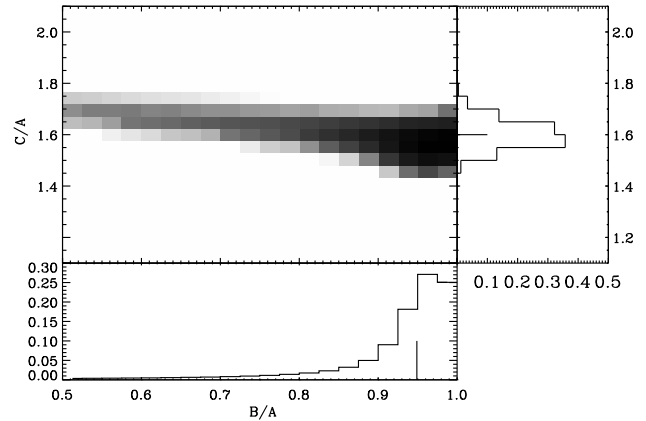


Figure 2. The distribution of the axial ratios of the bulge of NGC 4698. The median value of B/A and C/A is marked with a segment in the bottom and right-hand panel, respectively.

$$\phi_B = \arctan \frac{e \sin 2\delta}{\cos \theta (1 + e \cos 2\delta)} = 1^\circ.8, \quad (2)$$

$$\phi_C = \frac{1}{2} \arctan \frac{2e \sin 2\delta \cos \theta}{e \cos 2\delta (1 + \cos^2 \theta) - \sin^2 \theta} = 89^\circ.6. \quad (3)$$

Since the axial ratios B/A and C/A are both functions of the same variable ϕ , their probabilities are identical, i.e., for a given value of B/A with probability $P(B/A)$, the corresponding value of C/A obtained by Eq. 1 has a probability $P(C/A) = P(B/A)$. This allows to obtain the range of possible values of B/A and C/A for the bulge of NGC 4698 and to constrain its most probable intrinsic shape by adopting the probabilities $P(Z)$ and $P(F)$ derived by following MA+10. Fig. 2 shows the distribution of B/A and C/A calculated via Monte Carlo simulations. We randomly chose 5000 geometric configurations assuming a Gaussian distribution of q_b , q_d , PA_b , and PA_d taking into account their 3σ errors. For each geometric configuration we derived 1000 values of B/A and C/A according to their probability distribution functions (see MA+10). Therefore, the resulting median values of the axial ratios and the 3σ confidence intervals from their cumulative distribution are $B/A = 0.95^{+0.05}_{-0.91}$ and $C/A = 1.60^{+0.18}_{-0.12}$, respectively. The bulge of NGC 4698 is elongated orthogonal to the main disc and the probability that it has an equatorial section ($B/A < 0.95$) is 50 per cent.

3 THE NUCLEAR STELLAR DISC

3.1 Hubble Space Telescope imaging

The Wide Field Planetary Camera 2 (WFPC2) images of NGC 4698 obtained with the filters $F450W$ (Prop. Id. 9042, P.I. S. J. Smartt), $F606W$ (Prop. Id. 6359, P.I. M. Stiavelli), and $F814W$ (Prop. Id. 9042, P.I. S. J. Smartt) were retrieved from the *HST* Science Data Archive. The $F606W$ images were taken by centring the galaxy nucleus on the Planetary Camera (PC), whereas the others were taken with the Wide Field Camera (WFC). The PC and WFC detectors are Loral CCDs with 800×800 pixels and a pixel size of $15 \times 15 \mu\text{m}^2$. The PC image scale of 0.046 arcsec pixel $^{-1}$ yields a field of view of about 36×36 arcsec 2 . Each WFC detector covers 72×72 arcsec 2 with 0.091 arcsec pixel $^{-1}$. To help in identifying and correcting cosmic ray events, different exposures were

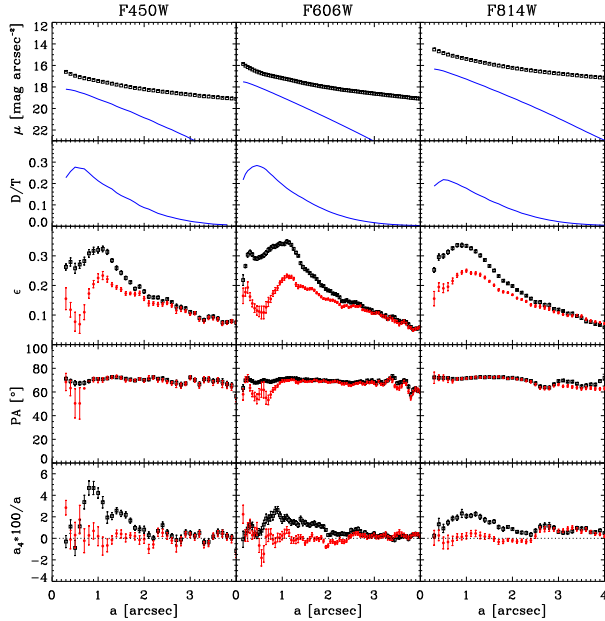


Figure 3. Isophotal parameters of the nuclear region of NGC 4698 as a function of the isophotal semi-major axis based on the analysis of the surface-brightness distribution measured in the *F450W* (left-hand panels), *F606W* (central panels), and *F814W* (right-hand panels) images, respectively. From top to bottom: Surface-brightness radial profiles of the galaxy (open black squares) and NSD (after convolution with the *HST* PSF, solid blue line). Radial profile of the NSD-to-total luminosity ratio. Radial profiles of the galaxy ellipticity, position angle, and fourth cosine Fourier coefficient before (open black squares) and after (filled red circles) the subtraction of the best-fitting model for the NSD.

taken with each filter. The total exposure times was 460 s for the *F450W* and *F814W* filters and 600 s for the *F606W* filter. The telescope was always guided in fine lock, giving a typical rms tracking error per exposure of 0.005 arcsec. The images were reduced using the CALWFPC reduction pipeline in IRAF (McMaster et al. 2008). Subsequent analysis including alignment and combination, rejection of cosmic rays, and sky subtraction was performed using IRAF standard tasks. The flux calibration to the Vega magnitude system was performed following Holtzman et al. (1995). The flux calibration to the Vega magnitude system in the *HST* passbands was performed following Holtzman et al. (1995).

Following Pizzella et al. (2002) the unsharp-masked image of each WFPC2 frame was built to first gauge the structure and extent of the NSD in all the available images. This procedure enhanced any surface-brightness fluctuation and non-circular structure extending over a spatial region comparable to the standard deviation of the smoothing Gaussian. The galaxy nucleus clearly reveals the presence of a highly elongated structure in all the images. This is the NSD and its location, orientation, and size are the same in all the observed passbands. This nuclear structure is associated with a central increase in ellipticity, ϵ , and fourth cosine Fourier coefficient, a_4 , as measured by performing an isophotal analysis using ELLIPSE and shown in Fig. 3.

The photometric parameters of the NSD were derived in the different passbands using the method by Scorza & Bender (1995, hereafter SB95) as implemented by Morelli et al. (2004) although with a different treatment of the PSF. The photometric decomposition was performed independently for each band-pass. The SB95

Table 1. Photometric parameters of the nuclear stellar disc.

Filter	$I_{0,\text{NSD}}$ [mag arcsec $^{-2}$]	h_{NSD} [pc]	i_{NSD} [$^{\circ}$]	PA_{NSD} [$^{\circ}$]
<i>F450W</i>	$17.39^{+0.24}_{-0.04}$	$50.4^{+1.8}_{-6.7}$	$79.4^{+3.3}_{-6.4}$	70 ± 2
<i>F606W</i>	$16.97^{+0.49}_{-0.12}$	$45.2^{+4.1}_{-6.0}$	$73.4^{+2.2}_{-4.7}$	71 ± 2
<i>F814W</i>	$15.63^{+0.45}_{-0.29}$	$50.4^{+9.8}_{-11.1}$	$75.5^{+9.0}_{-5.2}$	68 ± 2

method is based on the assumption that the isophotal disciness is the result of the superimposition of a host spheroidal component and an inclined exponential disc. Both the components are assumed to have perfectly elliptical isophotes with constant but different ellipticity. The method consists of the iterative subtraction of an infinitesimally thin disc model characterised by an exponential surface-brightness profile with central surface brightness $I_{0,\text{NSD}}$, scalelength h_{NSD} , axial ratio q_{NSD} , and position angle PA_{NSD} . The NSD parameters are adjusted until the departures from perfect ellipses are minimised (i.e., $a_4 \approx 0$). To properly derive the photometric parameters of the NSD, it is important to account for the *HST* PSF. For each nuclear disc model, the disc-free image of the galaxy was obtained from the galaxy image by subtracting the nuclear disc model after convolving with the *HST* PSF. The adopted PSF model was calculated with the TINYTIM package taking into account the instrumental setup and position of the NSD on the given image (Krist & Hook 1999). The best-fitting values of the NSD parameters and their 3σ errors were derived as in Morelli et al. (2004) and are listed in Tab. 1. The NSD inclination is calculated as $i_{\text{NSD}} = \arccos q_{\text{NSD}}$. The NSD is elongated like the galaxy bulge as is evident from its position angle. The comparison between the isophotal parameters of NGC 4698 measured before and after the subtraction of the best-fitting model of the NSD are shown in Fig. 3.

Pizzella et al. (2002) had already analysed the *F606W* image with the SB95 method. They deconvolved the galaxy image from the effects of the PSF using the Richardson-Lucy method. We decided to repeat the photometric decomposition since both an homogeneous photometric decomposition and an estimate of the errors on the fitted parameters are required to properly compare the structural parameters of the NSD in the different passbands. Moreover, this allowed us to verify that the NSD parameters obtained by subtracting the PSF-convolved disc model from the galaxy image are in agreement within the errors with those obtained by subtracting the unconvolved disc model from a deconvolved galaxy image. To this aim the conversion to Johnson *V* band has to be taken into account for a proper comparison of $I_{0,\text{NSD}}$ and was calculated with IRAF task SYNPHOT ($V - F606W = 0.27$ for a spiral galaxy).

3.2 Formation of the nuclear stellar disc

The structural parameters of the NSD (i.e., scalelength, inclination, and position angle) are constant within the errors in all the available WFPC2 images. Therefore, the location, orientation, and size of the NSD do not depend on the observed passband. This also implies the absence of colour gradients in the NSD, an important constraint on the star formation process. The mean values of the NSD parameters are $\langle h_{\text{NSD}} \rangle = 48.7$ pc, $\langle i_{\text{NSD}} \rangle = 76^{\circ}.1$, and $\langle \text{PA}_{\text{NSD}} \rangle = 69^{\circ}.7$. The size and luminosity are consistent with those of the other NSDs detected so far (see Ledo et al. 2010, for a census). The NSD is oriented as is the bulge, and its major axis is perpendicular to that of the main disc, i.e. it is a polar NSD.

A linear combination of single-age stellar population synthe-

sis models was used by Sarzi et al. (2005) to interpret an *HST* spectrum measured within the central 0.13 arcsec (11 pc) of NGC 4698. The continuum spectral energy distribution between 3000-5700 Å was best fitted by a very old stellar population (10 Gyr) with no evidence for stars younger than 5 Gyr in the galaxy nucleus, where the NSD light contamination is large (~ 20 per cent, Fig. 3). The light fraction from stars younger than 1 Gyr rises to 2 per cent if supersolar-metallicity models are considered. This implies that the centre of the NSD is made mostly of old stars. Models for chemical and spectro-photometric evolution of galaxy discs predict a strong evolution with age of their colour profiles as direct consequence of an inside-out formation (Boissier & Prantzos 1999; Prantzos & Boissier 2000). In this scenario colour gradients are produced early on in the disc centre and propagate outwards. The maximum colour gradient measured for the NSD ($|d(B - R)/dr| < 0.05 \text{ mag kpc}^{-1}$) falls short of the model predictions and it is not consistent with a picture wherein the nuclear disc assembled inside out in the last 5-10 Gyr.

4 DISCUSSION AND CONCLUSIONS

The structure of the nucleus and bulge of the Virgo spiral galaxy NGC 4698 was investigated through a detailed analysis of *HST* optical and UKIRT near-infrared images, respectively. The galaxy is known to host a nuclear disc of gas and stars which is rotating perpendicularly with respect to the galaxy main disc. Moreover, the bulge and main disc appear on the sky elongated perpendicular to each other (Bertola et al. 1999; Bertola & Corsini 2000; Pizzella et al. 2002).

The equatorial ellipticity and intrinsic flattening of the polar bulge were obtained following MA+10 from the apparent ellipticity of the bulge, twist angle between the bulge and main disc, and main disc inclination measured in the UKIDSS near-infrared image by adopting the photometric decomposition method by MA+08. The bulge of NGC 4698 is remarkably elongated in a perpendicular direction with respect to the disc plane ($C/A = 1.60^{+0.18}_{-0.12}$). Although the consistency with axisymmetry was recognised ($B/A = 0.95^{+0.05}_{-0.91}$), still the probability that it is significantly triaxial (i.e., with an equatorial elliptical section with $B/A < 0.95$) is 50 per cent. The central surface brightness, scalelength, inclination, and position angle of the polar NSD in all the available *HST* images were measured by assuming it is an infinitesimally thin exponential disc and applying the photometric decomposition method of SB95 as implemented by Morelli et al. (2004). The size, orientation, and location of the polar NSD do not depend on the observed passband, as already observed for the few other NSDs for which a detailed multi-band photometric analysis was performed (Krajinović & Jaffe 2004; Morelli et al. 2010).

The combination of these new results about the complex structure of NGC 4698 gives us the opportunity to gain further insight on the formation of NSDs with the goal of motivating numerical modelling to test and refine this scenario. The kinematical decoupling between two components of a galaxy suggests the occurrence of an accretion event or merging (Bertola & Corsini 1999). Therefore, it is straightforward to explain the existence of the orthogonally-rotating dynamically-cold nuclear disc in NGC 4698 as the end result of the acquisition of external gas by the pre-existing galaxy. Gas dissipation is indeed a necessary ingredient since purely stellar dynamical mergers can not form a nuclear disc (Hartmann et al. 2011). In NGC 4698 the accreted gas settled on the principal plane perpendicular to the shortest axis of the triaxial bulge (i.e., perpen-

dicular to the galaxy main disc) and formed stars. The major axis of the NSD is elongated in the same direction as the bulge. The link between the angular momentum transport from galactic to nuclear scales and formation of NSDs has been recently investigated by Hopkins & Quataert (2010). The stellar population in the centre of NGC 4698 is very old (Sarzi et al. 2005). The absence of colour gradients in the NSD is explained if either the star formation homogeneously occurred all over the extension of the disc or the NSD assembled through an inside-out process that ended more than 5 Gyr ago.

ACKNOWLEDGMENTS

We are grateful to Victor P. Debattista for valuable comments. This work is supported by Padua University (grant 60A02-1283/10) and Italian Space Agency (contract ASI-INAF I/009/10/0). LM acknowledges support from Padua University (grant CPS0204). JMA is partially funded by the Spanish MICINN (Consolider-Ingenio 2010 Program grant CSD2006-00070 and grants AYA2007-67965-C03-01 and AYA2010-21887-C04-04).

REFERENCES

- Bertola F., Corsini E. M., 1999, in Barnes J. E., Sanders, D. B., eds, IAU Symp. 186, Galaxy Interactions at Low and High Redshift, Kluwer, Dordrecht, p. 149
- Bertola F., Corsini E. M., 2000, in Combes F., Mamon G. A., Charmandaris V., eds, ASP Conf. Ser. 197, Dynamics of Galaxies: from the Early Universe to the Present, Astron. Soc. Pac., San Francisco, p. 115
- Bertola F., Vietri M., Zeilinger W. W., 1991, ApJ, 374, L13
- Bertola F., Corsini E. M., Vega Beltrán J. C., Pizzella A., Sarzi M., Cappellari M., Funes J. G., 1999, ApJ, 519, L127
- Boissier S., Prantzos N., 1999, MNRAS, 307, 857
- Cappellari M., et al., 2006, MNRAS, 366, 1126
- Coccatto L., Corsini E. M., Pizzella A., Morelli L., Funes J. G., Bertola F., 2004, A&A, 416, 507
- Corsini E. M., et al., 1999, A&A, 342, 671
- de Vaucouleurs G., de Vaucouleurs A., Corwin H. G., Jr., Buta R. J., Paturel G., Fouque P., 1991, Third Reference Catalogue of Bright Galaxies, Springer-Verlag, Berlin (RC3)
- Falcón-Barroso J., et al., 2006, MNRAS, 369, 529
- Fathi K., Peletier R. F., 2003, A&A, 407, 61
- Freedman W. L., et al., 1994, Nature, 371, 757
- Hambly N. C., et al., 2008, MNRAS, 384, 637
- Hartmann M., Debattista V. P., Seth A., Cappellari M., Quinn T. R., 2011, MNRAS, 418, 2697
- Holtzman J. A., et al., 1995, PASP, 107, 156
- Hopkins P. F., Quataert E., 2010, MNRAS, 405, L41
- Kassin S. A., de Jong R. S., Pogge R. W., 2006, ApJS, 162, 80
- Kormendy J., Kennicutt R. C., Jr., 2004, ARA&A, 42, 603
- Krajinović D., Jaffe W., 2004, A&A, 428, 877
- Krist J., Hook R., 1999, STIS Instrument Handbook, Version 4.0, STScI, Baltimore
- Lawrence A., et al., 2007, MNRAS, 379, 1599
- Ledo H. R., Sarzi M., Dotti M., Khochfar S., Morelli L., 2010, MNRAS, 407, 969
- Lindblad B., 1956, Stockholms Observatoriums Annaler, 19, 7
- Matthews L. D., de Grijs R., 2004, AJ, 128, 137

- McMaster M., et al. 2008, WFPC2 Instrument Handbook, Version 10.0, STScI, Baltimore
- Méndez-Abreu J., Aguerri J. A. L., Corsini E. M., Simonneau E., 2008, *A&A*, 478, 353 (MA+08)
- Méndez-Abreu J., Simonneau E., Aguerri J. A. L., Corsini E. M., 2010, *A&A*, 521, A71 (MA+10)
- Möllenhoff C., Heidt J., 2001, *A&A*, 368, 16
- Morelli L., et al., 2004, *MNRAS*, 354, 753
- Morelli L., Cesetti M., Corsini E. M., Pizzella A., Dalla Bontà E., Sarzi M., Bertola F., 2010, *A&A*, 518, A32
- Pignatelli E., et al., 2001, *MNRAS*, 323, 188
- Pizzella A., Corsini E. M., Morelli L., Sarzi M., Scarlata C., Stivelli M., Bertola F., 2002, *ApJ*, 573, 131
- Prantzos N., Boissier S., 2000, *MNRAS*, 313, 338
- Sarzi M., Corsini E. M., Pizzella A., Vega Beltrán J. C., Cappellari M., Funes J. G., Bertola F., 2000, *A&A*, 360, 439
- Sarzi M., Rix H.-W., Shields J. C., Ho L. C., Barth A. J., Rudnick G., Filippenko A. V., Sargent W. L. W., 2005, *ApJ*, 628, 169
- Scorza C., Bender R., 1995, *A&A*, 293, 20 (SB95)
- Zaritsky D., Lo K. Y., 1986, *ApJ*, 303, 66